Quantum control via the dynamic Stark effect: application to switched rotational wave packets and molecular axis alignment

Sussman, Benjamin J.; Underwood, Jonathan G.; Lausten, R.; Ivanov, Misha Yu.; Stolow, Albert

Publisher's version / Version de l'éditeur:
https://doi.org/10.1103/PhysRevA.73.053403
Physical Review. A, Atomic, Molecular, and Optical Physics, 73, 5, pp. 053403-053414, 2006-04-30

Quantum control via the dynamic Stark effect: Application to switched rotational wave packets and molecular axis alignment

Benjamin J. Sussman,[1,2] Jonathan G. Underwood,[3] R. Lausten,[1,2] Misha Yu. Ivanov,[1] and Albert Stolow[1,2,*]
[1]*Steacie Institute for Molecular Sciences, National Research Council of Canada, 100 Sussex Drive, Ottawa, Ontario, Canada K1A 0R6*
[2]*Department of Physics, Queen's University, Kingston, Ontario, Canada K7L 3N6*
[3]*Department of Physics and Astronomy, The Open University, Walton Hall, Milton Keynes, MK7 6AA, United Kingdom*
(Received 1 February 2006; published 5 May 2006)

Nonperturbative quantum control schemes in the intermediate field strength (nonionizing) regime are investigated. We restrict the matter-field interaction to the nonresonant dynamic Stark effect (NRDSE) as induced by infrared laser fields, which we argue is a new and general tool for quantum control of atomic and molecular dynamics. For the case of Raman coupled matter states, an effective Hamiltonian may be constructed, and quantum control via NRDSE may be thought of as reversibly modifying the effective Hamiltonian during system propagation, thus leading to control over dynamic processes. As an illustration, the creation of field-free "switched" wave packets through the adiabatic turn on and sudden turn off of the NRDSE is considered and experimentally demonstrated. Wave packets generated through the switched NRDSE interaction may be very different in form and content than wave packets generated via resonant transitions with Gaussian optical pulses. In order to provide an example, we discuss the specific case of rotational wave packet dynamics where the NRDSE manifests itself as molecular axis alignment. This technique is applied to the creation of field-free molecular axis alignment using an intense switched 1.064 μm laser pulse. This switched laser pulse was generated via a plasma shuttering technique, giving a pulse with a rise time of 150 ps and a fall time of 170 fs. The temporal evolution of the molecular axis alignment is probed via the optical Kerr effect. Field-free alignment via the switched NRDSE is demonstrated for both linear (CO_2, CS_2) and symmetric top (1,2-propadiene) polyatomic molecules.

DOI: 10.1103/PhysRevA.73.053403 PACS number(s): 32.80.Qk, 42.50.Hz

I. INTRODUCTION

Modern quantum control began with the development of coherent optical phase control schemes based upon the interference between two or more pathways to a target eigenstate [1–4]. Although these coherent control schemes were initially based upon a perturbative description of the field-matter interaction, schemes using strong resonant or near-resonant laser fields soon followed [5–7]. An alternative approach based upon the nonlinear interaction of an adaptively shaped femtosecond laser pulse using feedback-learning algorithms to optimize a chosen product was also proposed [8]. This was most successfully demonstrated in the strong field fragmentation ionization of polyatomic molecules [9,10] and atomic ionization [11] and exploits the large coherent bandwidth intrinsic to femtosecond laser pulses. These schemes are nonperturbative in that a series expansion solution in the interaction strength may not be pertinent, and that they may involve many complex processes including multiphoton resonances, dynamic Stark effects, propagation on multiple potential energy surfaces and strong field ionization-fragmentation processes [12–15]. In such situations, it can be difficult to discern which mechanisms dominate. At lower (nonionizing) intensities, strong shaped pulses have been used to control processes in condensed phases [16,17] and again may involve multiphoton resonances and dynamic Stark effects, as well as nonlinear propagation effects. In the perturbative limit, pulse shaping predictably alters nonlinear power spectra, leading to changes in resonant multiphoton transition probabilities [18,19]. In general, however, although the underlying mechanisms are complex and difficult to elucidate, strong field shaped pulse feedback control has been a successful control technique.

In view of the need to disentangle the complex mechanisms associated with strong field quantum control, this paper considers a nonperturbative control scheme dependent exclusively upon only one of these mechanisms: the nonresonant dynamic Stark effect (NRDSE). Ionization adds several well known but complex physical phenomena to the control mechanisms [12–15] and therefore discussions here are restricted to nonionizing laser fields. Furthermore, this discussion is restricted to NRDSE control of nuclear dynamics on a single electronic potential energy surface for which it is necessary to avoid electronic excitation altogether. To this end, the carrier frequencies employed should lie in the infrared region, well away from any low order resonances. Despite these two restrictions, we note that NRDSE couples field-free eigenstates in a manner very different from resonant or near-resonant excitation, thus providing a unique route to quantum control. The nonresonant nature of this scheme conveniently removes the details of the carrier frequency from the problem: there is no requirement to tune the laser frequency to match transitions in a system.

As discussed elsewhere [20], the coupling of field-free states via NRDSE can be divided into two limiting cases. If the dipole coupling of neighboring eigenstates dominates,

*Electronic address: albert.stolow@nrc.ca

then the coherent superposition in the field attempts to oscillate at the laser pulse carrier frequency. By contrast, if the Raman coupling of neighboring eigenstates through electronic states far off resonance dominates, then the coherent superposition in the laser field follows the envelope of the laser pulse. In this case, the contribution of the effects of all far off-resonance states may be treated as a polarizability and an effective Hamiltonian may be constructed. One of the central points of this paper is that the NRDSE allows for dynamic yet reversible control of this effective Hamiltonian *during* the system propagation.

In the following we consider the use of NRDSE to modify the effective Hamiltonians of molecular systems. Elsewhere, we discuss the use of NRDSE to control vibronic dynamics and photodissociation branching ratios in molecular systems [21]. In this paper, the control of rotational dynamics and axis alignment of molecular systems is investigated. In this case the field-free Hamiltonian has angular invariance, and application of a NRDSE laser pulse creates a potential well along the laser polarization direction. Control over the time-dependent depth or even direction of this well amounts to controlling the system propagator during propagation. As a demonstration of this principle, we consider the use of NRDSE laser fields to produce characteristic superpositions of field-free rotational states which lead to field-free molecular axis alignment [22,23]. By rapidly truncating an adiabatically applied NRDSE interaction, it is possible to project the laser field prepared state onto the field-free basis, thus creating a switched rotational wave packet. Observing the subsequent evolution of the wave packet prepared in this manner provides detailed insight into the interaction of the molecular system with the nonperturbative laser field.

There is current interest in molecular axis alignment because it offers the ability to bring the molecular frame, where molecular processes occur, into the laboratory frame where measurements are made. This will advance emerging techniques for the study of molecular structure and dynamics where orientational averaging of the molecular frame leads to a considerable loss of information. Examples include time-resolved photoelectron spectroscopy [24–26], time-resolved x ray [27–29], electron diffraction [30,31], and timed Coulomb explosion [15,32].

Additional interest in molecular alignment stems from recent work which shows that the emission of high harmonics from molecular gases depends upon the molecular orientation and may be strongly enhanced for an aligned ensemble [33]. From these measurements it is clear that the high harmonic spectra observed from such aligned samples contain signatures of the molecular structure [34,35]. However, in order to probe native structure and dynamics, the measurements must be made field free, in the absence of the intense alignment laser field which strongly perturbs the system. In this paper we show how this may be achieved by the use of an adiabatically applied and suddenly truncated NRDSE interaction: the rotational wave packet that arises will exhibit revival structure and hence transient field-free axis alignment.

Beyond the microscopic applications of molecular alignment, there are also many macroscopic prospects. The axis alignment produces a transient birefringence in the target medium and, below, we show that this allows the optical Kerr effect (OKE) to monitor the evolution of the rotational wave packet. Recently, the time-dependent birefringence associated with recurring molecular axis alignment has been used for phase matching of nonlinear optical processes [36] and pulse compression [37]. This is an example of using shaped laser pulses to control molecular dynamics which in turn effects macroscopic characteristics and it will surely find many more applications as improved techniques are developed.

This paper is organized as follows: in Sec. II we discuss the nonresonant dynamic Stark effect and introduce the effective Hamiltonian method as a means of inducing quantum control. The dipole dominated and the Raman dominated regime are contrasted. Section III introduces the idea of adiabatic preparation and sudden truncation and the general case is specialized to rotational alignment. Section IV discusses the implementation of the plasma shutter which is used to abruptly truncate a 150 ps pulse in 170 fs, thus producing the switched control pulse. The induced molecular axis alignment is observed using the optical Kerr effect, the details of which are discussed in Sec. V. In Sec. VI we experimentally demonstrate control over molecular alignment using the NRDSE in both linear (CO_2, CS_2) and symmetric top polyatomic (1,2-propadiene) molecules. We conclude with a summary and a discussion of future prospects.

II. THE NONRESONANT DYNAMIC STARK EFFECT AND SWITCHED WAVE PACKETS

When studying the dynamics of a quantum system under the influence of electromagnetic fields that are nondestructive, it is common to find that systems naturally partition into two sets of states: a set that participates in the dynamics directly, and a set with negligible population that mediates the dynamics by coupling the populated states in the presence of the nonresonant laser field. We shall refer to these as the essential (E) and nonessential states (N) respectively [38]. Often, E corresponds to the ground molecular electronic state and N corresponds to all excited states. By "integrating out" the motion in N, the dynamics in E can be understood by introducing a polarizability whose contribution comes from the coupling of E via N. For laser fields, the system dynamics have two different limits: (i) the dipole limit, where dipole coupling between E states dominates, and (ii) the Raman limit, where the polarizability due to the coupling via N states dominates.

To develop the two limits, the following convention for state indices is introduced: $\{\ell, m \in E \cup N\}$, $\{j, k \in E\}$, and $\{p \in N\}$ (see Fig. 1). The interaction with a strong laser field of the form

$$\mathbf{E}(t) = \tfrac{1}{2}\boldsymbol{\mathcal{E}}(t)e^{-i\omega t} + \text{c.c.} \tag{1}$$

is given by

$$V(t) = -\boldsymbol{\mu} \cdot \mathbf{E}(t) \tag{2}$$

where $\boldsymbol{\mu}$ is the dipole moment of the system, $\boldsymbol{\mathcal{E}}(t)$ is the pulse envelope, and ω is the laser carrier frequency.

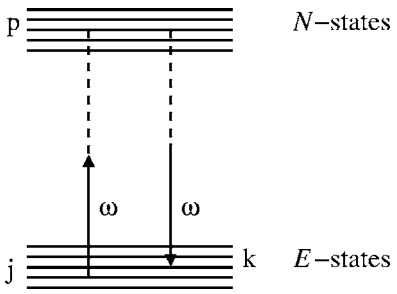

FIG. 1. Transitions between levels j and k within the E manifold of states are mediated by far off-resonance transitions via p states in the N manifold (Raman transitions), as well as by direct dipole coupling. The N manifold of states contributes to the Raman polarizability. See text for further details.

Expansion of the wave-function in terms of the field free basis

$$|\Psi(t)\rangle = \sum_{\ell} c_l(t) e^{-i\omega_\ell t} |l\rangle \tag{3}$$

and substitution into the time-dependent Schrödinger equation yields the equations of motion of the system

$$i\hbar \dot{c}_\ell = \sum_m e^{-i\omega_{m\ell} t} V_{\ell m}(t) c_m(t) \tag{4}$$

where

$$\omega_{m\ell} = \omega_m - \omega_\ell, \tag{5}$$

and

$$V_{\ell m}(t) = \langle \ell | \boldsymbol{\mu} \cdot \mathbf{E}(t) | m \rangle. \tag{6}$$

Assuming there is no initial population in N and that there are no intra-N processes, the N dynamics can be written as

$$c_p(t) = \frac{1}{i\hbar} \int_{-\infty}^{t} dt \sum_j e^{-i\omega_{jp} t} V_{pj}(t) c_j(t). \tag{7}$$

Integrating by parts repeatedly yields

$$c_p(t) = -\frac{1}{2\hbar} \sum_{s=0}^{\infty} \sum_j (-i)^s \frac{e^{-i(\omega_{jp}-\omega)t}}{(\omega_{jp}-\omega)^{s+1}} \frac{d^s}{dt^s} (\boldsymbol{\mathcal{E}}(t) c_j(t)) \cdot \boldsymbol{\mu}_{pj} + [\omega \to -\omega, \boldsymbol{\mathcal{E}}(t) \to \boldsymbol{\mathcal{E}}(t)^*], \tag{8}$$

where $\boldsymbol{\mu}_{pj} = \langle p | \boldsymbol{\mu} | j \rangle$. Provided that the series in s converges rapidly, it is sufficient to keep only the $s=0$ term. However, for rapidly varying envelopes, $s>0$ terms must be included.

For the present case, the $s=0$ term may now be inserted into the equations of motion for the E states. The rotating wave approximation is then invoked by neglecting the fast moving oscillations, whose contributions are not cumulative. Thus, the dynamics for the E states may be written as

$$i\hbar \dot{c}_k = \sum_j e^{-i\omega_{jk} t} V^e_{kj}(t), \tag{9}$$

where the effective perturbation $V^e_{kj}(t) = V^d_{kj}(t) + V'^R_{kj}(t)$ is composed of a dipole contribution

$$V^d_{kj}(t) = -\boldsymbol{\mu}_{kj} \cdot \mathbf{E}(t) \tag{10}$$

and a Raman contribution

$$V^R_{kj}(t) = -\frac{1}{4} \sum_p \left(\frac{\boldsymbol{\mu}_{kp} \cdot \boldsymbol{\mathcal{E}}^*(t) \boldsymbol{\mu}_{pj} \cdot \boldsymbol{\mathcal{E}}(t)}{\omega_{pj} + \omega} + \frac{\boldsymbol{\mu}_{kp} \cdot \boldsymbol{\mathcal{E}}(t) \boldsymbol{\mu}_{pj} \cdot \boldsymbol{\mathcal{E}}^*(t)}{\omega_{pj} - \omega} \right). \tag{11}$$

It is important to note that when the dipole coupling dominates the dynamics follow instantaneous field, and when the Raman coupling dominates the dynamics only follow the field envelope. Equation (11) can be written as

$$V^R_{kj}(t) = -\tfrac{1}{4} \boldsymbol{\mathcal{E}}^*(t) \cdot \boldsymbol{\alpha}_{kj} \cdot \boldsymbol{\mathcal{E}}(t), \tag{12}$$

where the Cartesian components of the Raman polarizability are

$$\alpha^{ab}_{kj} = \sum_p \left(\frac{\mu^a_{kp} \mu^b_{pj}}{\omega_{pj} + \omega} + \frac{\mu^b_{kp} \mu^a_{pj}}{\omega_{pj} - \omega} \right) \tag{13}$$

with $\{a, b \in x, y, z\}$. To proceed we consider the molecular case and separate the index k into nuclear and electronic components

$$k \to e, n, \tag{14a}$$

$$|k\rangle \to |\phi_n(R)\rangle |\psi_e(r;R)\rangle, \tag{14b}$$

where $|\phi^n(R)\rangle$ is the rovibrational wave function of the e electronic state characterized by the set of nuclear quantum numbers n dependent upon the nuclear coordinates R, and $|\psi_e(r;R)\rangle$ is the electronic wave function dependent upon the electronic coordinate r, and parametrically dependent upon the nuclear coordinates R. The nuclear and electronic separation allows the polarizability to be written as

$$\alpha^{ab}_{e_1 n_1, e_2 n_2} = \sum_{e_3 n_3 \in N} \left(\frac{\mu^a{}_{e_1 n_1, e_3 n_3} \mu^b{}_{e_3 n_3, e_2 n_2}}{\omega_{e_3 n_3, e_2 n_2} + \omega} + \frac{\mu^b{}_{e_1 n_1, e_3 n_3} \mu^a{}_{e_3 n_3, e_2 n_2}}{\omega_{e_3 n_3, e_2 n_2} - \omega} \right). \tag{15}$$

This paper is only concerned with dynamics on a single ground electronic state $e_1 = e_2$. Since the electronic response of the molecule dominates the interaction, the polarizability varies very little with nuclear quantum numbers n_2 and n_3. Under conditions where we may neglect the dependence of the denominator of (15) upon n_2 and n_3, the nuclear closure identity can be used to write the Raman polarizability as

$$\alpha^{ab}_{e_1} = \sum_{e_3 \in N} \left(\frac{\mu^a{}_{e_1,e_3}\mu^b{}_{e_3,e_1}}{\bar{\omega}_{e_3,e_1} + \omega} + \frac{\mu^b{}_{e_1,e_3}\mu^a{}_{e_3,e_1}}{\bar{\omega}_{e_3,e_1} - \omega} \right), \tag{16}$$

where the denominators in (15) have been replaced by an average electronic energy level splitting, $\bar{\omega}_{e_3,e_1}$. Raman type rotational transitions within the e_1 are then described by

$$V^R_{n_1 n_2}(t) = -\tfrac{1}{4}\langle \phi_{n_1}(R)|\boldsymbol{\mathcal{E}}^*(t)\cdot\boldsymbol{\alpha}_{e_1}\cdot\boldsymbol{\mathcal{E}}(t)|\phi_{n_2}(R)\rangle. \tag{17}$$

For ground electronic state dynamics, in many cases it is appropriate to approximate (16) by the usual static polarizability.

In the presence of a strong, nonresonant, but nondestructive laser field two limits of coupling therefore exist: the dipole limit (10) and the Raman limit (17). Which limit applies depends on the particular matrix elements and detunings. In the dipole case the dynamics follow the instantaneous electric field, whereas in the Raman case the dynamics follow the field envelope leading to the general idea of reversibly modifying the molecular Hamiltonian during its evolution. For the remainder of this paper we shall consider the limiting case of Raman coupling of rotational states.

In the Raman limit, if the optical envelope varies sufficiently slowly, the system evolution will be adiabatic. A nonadiabatic change of conditions is therefore required to leave any modification of eigenstate amplitudes and phases after the laser pulse; a pulse which turns adiabatically on and off will leave an eigenstate unchanged, up to a phase. In this paper we consider the effect of an adiabatically applied and suddenly truncated laser field.

If the interaction with the laser field is turned on sufficiently slowly that the system is able to adjust continuously and reversibly, each field free eigenstate will evolve into a single adiabatic dressed state, which are solutions of the instantaneous stationary Schrödinger equation with time treated as a parameter [39,40]

$$[H_0 + V^R(t)]|\phi_n(R;t)\rangle = E_n(t)|\phi_n(R;t)\rangle, \tag{18}$$

where $|\phi_n(R;t)\rangle$ is the instantaneous eigenstate with energy $E_n(t)$ which correlates to the field free eigenstate $|\phi_n(R;0)\rangle$ in the absence of the applied field at $t=0$. These states are themselves superpositions of field free eigenstates. In this paper we consider the case where the interaction is turned on adiabatically, which provides the simplest field induced dynamics and also poses the advantage that the ground state will exhibit the greatest localization in the conjugate variable (although, a carefully phased superposition of dressed states may give higher localization). If the pulse is switched off instantaneously at time t_{sw} (the sudden limit), the field free superposition after the field turns off will be identical to that at the peak of the field and subsequent evolution will be governed by the field free Hamiltonian. Assuming the laser field was turned on adiabatically forming a single dressed state, the resulting nuclear wave packet is described by

$$|\psi(t < t_{sw})\rangle = e^{-i\int_0^t E_n(t)dt}|\phi_n(R;t)\rangle, \tag{19}$$

$$|\psi(t > t_{sw})\rangle = e^{-i\int_0^{t_{sw}} E_n(t)dt}\sum_m |\phi_m(R;0)\rangle A^n_m(t_{sw})e^{i\Phi^n_m(t_{sw})-iE_n(0)t}, \tag{20}$$

where $A^n_m(t_{sw})e^{i\Phi^n_m(t_{sw})}$ is the coefficient of the field free state m that correlates to starting in state n. $A^n_m(t_{sw})$ is real and $\Phi^n_m(t_{sw})=$const for a particular n [39]. The subsequent time evolution of this superposition state will directly reflect the field induced mixing of the eigenstates and so will reveal important information about the interaction of the intense field with the system. The revivals of this superposition will also exhibit similar localization to the field induced state. In the case of the alignment of rotors (discussed below) in which transitions are induced between molecular rotational states, an adiabatic application and sudden truncation of (17) can be used for producing field free molecular alignment at the revival times of the rotational wave packet.

III. SWITCHED WAVE PACKETS AND MOLECULAR AXIS ALIGNMENT

A symmetric top molecule with $\alpha^{xx}=\alpha^{yy}\equiv\alpha_\perp$ and $\alpha^{zz}=\alpha_\parallel$ in the molecular (principle axis) frame (MF) when exposed to a nonresonant linearly polarized laser field of the form

$$\boldsymbol{E}(t) = \mathcal{E}(t)\cos(\omega t)\hat{z} \tag{21}$$

will experience an aligning potential in the laboratory frame (LF) due to a Raman interaction of the form (17). Explicitly expressing the geometrical dependence of the double dot product in (17) in terms of the Euler angles connecting the LF and MF [41], this interaction potential takes the form [22]

$$V^R(\theta,t) = -\tfrac{1}{4}\mathcal{E}^2(t)[(\alpha_\parallel - \alpha_\perp)\cos^2\theta + \alpha_\perp], \tag{22}$$

where θ is the angle between the laser polarization and the molecular axis, and $\mathcal{E}(t)$ is the slowly varying pulse envelope. The zero point contribution $-\frac{1}{4}\mathcal{E}^2(t)\alpha_\perp$ only contributes a net phase and can be ignored if calculations are only concerned with a case where relative phase between different systems is inconsequential. The nonresonant laser field will tend to induce alignment of the molecular z axis along the electric field direction (for $\alpha_\parallel > \alpha_\perp$). The dressed eigenstates of the resultant Hamiltonian are referred to as pendular states, and each pendular state may be decomposed as a superposition of field free molecular rotational eigenstates. As long as the rise of the laser pulse envelope is adiabatic with respect to molecular rotations, each field free eigenstate will evolve adiabatically into a single pendular state. If the laser pulse envelope is turned off adiabatically, no axis alignment persists. However, if the aligning pulse is suddenly truncated, a superposition of field free rotational states is created which will exhibit wave packet evolution after the laser pulse. The revivals of this wave packet will exhibit field-free alignment equivalent to that at the instant of laser pulse truncation.

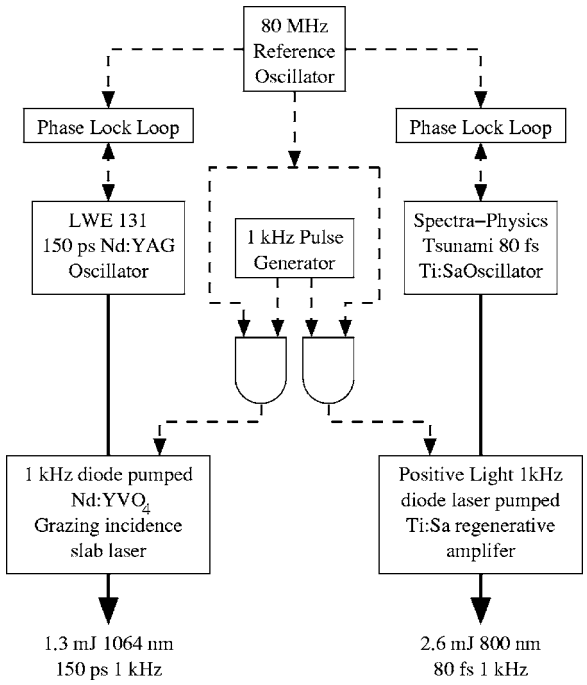

FIG. 2. Schematics of the laser system and synchronization electronics. See text for further details.

IV. GENERATING SWITCHED LASER PULSES

We describe here a method of producing shaped laser fields with slow rise times and fast fall times. With current pulse spatial light modulators [42], the achievable truncation time is limited by the frequency content of the input laser pulse. Furthermore, it becomes increasingly challenging to create laser pulses which have both extremely long and extremely short temporal features owing to conjugate relationships that exist between the maximum temporal window and the finest achievable spectral feature (or alternatively, the total bandwidth and the shortest temporal feature) [43]. The time-dependent nature of the plasma shutter technique introduces spectral bandwidth that allows for the creation of fall times much more rapid than the input laser pulse would otherwise permit.

Plasma shutters have previously been used for the rapid truncation of deep infrared laser pulses [44] as well as vacuum ultraviolet (VUV) pulses [45] using solid media for the formation of the plasma. However, such methods are limited both in terms of the usable wavelengths and the intensity of the laser pulses being switched by the intrinsic damage threshold of the solid materials. The plasma shutter method detailed here utilizes an optically flat liquid jet for plasma generation which circumvents the limitations imposed by material damage as the liquid is replenished between laser shots. This method is readily scalable to higher laser intensities.

Two synchronized laser systems were used to produce the switched laser pulse (Fig. 2). A picosecond Nd:YAG oscillator (Lightwave Electronics, Model 131, 1.064 μm, 140 mW, 150 ps) and a femtosecond Ti:Sapphire oscillator (Spectra-Physics, Tsunami, 800 nm, 800 mW, 80 fs) were locked to an external 80 MHz reference crystal oscillator (Spectra-Physics 3930) using commercial phase locked loop electronics. The timing jitter between these two optical oscillators was <1 ps. The Nd:YAG oscillator was modified by installing an etalon in order to stretch the pulse duration to 150 ps. Amplification of the 1.064 μm Nd:YAG pulse was performed in a homebuilt 1 kHz $Nd:YVO_4$ diode pumped grazing incidence slab laser producing 1.064 μm, 150 ps, 1.3 mJ pulses [46]. The 800 nm pulse was amplified at 1 kHz in a two stage commercial chirped pulse amplifier system comprised of regenerative amplifier followed by a two pass amplifier (Positive Light Spitfire) to produce 80 fs pulses at 800 nm with 2.6 mJ energy per pulse. Synchronization of the two amplifiers was achieved by triggering the Pockels cells inside the cavities of both amplifiers from the same 1 kHz pulse generator. For each amplifier, the 1 kHz signal was used to set an "and" gate. The Pockels cells were then triggered within this gate by the 80 MHz reference oscillator. For the Positive Light amplifier, this was achieved using the commercial synchronization and a delay generator. For the homebuilt $Nd:YVO_4$ amplifier, the shorter cavity length required higher timing precision and the Pockels cell triggering was achieved with a 300 MHz discriminator unit (Phillips Scientific Model 6904). The coarse timing between the two lasers was set by adjusting the relative phase of the 80 MHz reference signal for the Ti:Sapphire phase lock loop relative to that for the Nd:YAG phase lock loop.

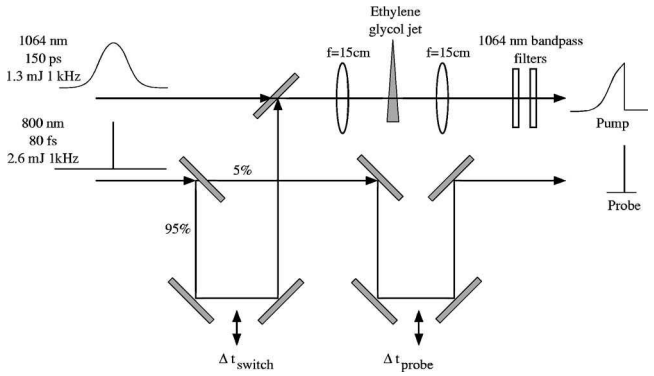

FIG. 3. Optical arrangement used for the creation of a switched laser pulse with a rise time of 150 ps, and a fall time of 170 fs. A probe beam synchronized to the falling edge of the switched pulse is obtained by splitting off part of the 800 nm beam prior to the plasma switch.

The optical arrangement used for creating the switched laser pulse is detailed in Fig. 3. A portion of the 800 nm beam (1.2 mJ) was copropagated with the 1.064 μm beam. These two beams were temporally and spatially centered with respect to each other, and both beams were focused onto the liquid jet with an $f=150$ mm lens. The ethylene glycol liquid jet was produced using a cooled recirculating laser dye jet system producing a ~ 100 μm thick jet which was optically flat across both foci. At the focus, the peak intensity of the 1.064 μm beam was $\sim 5\times 10^{11}$ W cm^{-2} (insufficient to cause breakdown) whereas the peak intensity of the 800 nm beam was $\sim 5\times 10^{14}$ W cm^{-2}, well above the threshold for breakdown. By timing the 800 nm pulse to arrive at the peak of the 1.064 μm pulse, the plasma generated by the 800 nm pulse was used to truncate the transmission of the 1.064 μm

light. Following the arrival of the 800 nm pulse, the plasma was driven and maintained by further absorption of energy from the 1.064 μm beam and absorption/reflection continued, as will be discussed below. The diameter of the 1.064 μm beam at the focusing lens was larger ($\sim$10 mm) than that of the 800 nm beam ($\sim$6 mm) such that the 800 nm spot was larger than the 1.064 μm spot at the focus, thus ensuring uniform truncation across the spatial profile. Following the ethylene glycol jet, the switched 1.064 μm pulse was recollimated with a second $f=150$ mm lens.

The high intensity 800 nm pulse produces a partially ionized plasma in the liquid jet with electron density N_e. In a collisionless plasma (modeled as a driven harmonic oscillator) the refractive index is given by

$$n = n_0\left(1 - \frac{N_e}{N_c}\right)^{1/2}, \tag{23}$$

where N_c is the critical density

$$N_c = \frac{\omega^2 m n_0}{4\pi e^2} = 1.1 \times 10^{21}\ \mathrm{cm}^{-3}. \tag{24}$$

N_c is the plasma electron density above which the medium begins to absorb, m is the electron mass, e is the electron charge, ω is the optical frequency of the ps pulse, and n_0 is the field free refractive index. Below the critical density, the intensity profile at the focal plane induces a radial charge carrier variation that behaves as a divergent optical "lens" for the 1.064 μm light, defocusing the copropagating pulse. Above the critical intensity, the aft portion of the 1.064 μm ps pulse is simultaneously absorbed and defocused as it propagates through the plasma in the ethylene glycol jet.

The plasma charge density N_e depends sensitively upon the absolute intensity at the focus and the details of the ionization dynamics of the liquid. While there are unresolved details on the precise mechanism of the plasma generation processes [47], a simple rate equation has been developed to estimate plasma production in the the presence of multiphoton and avalanche ionization [48]. The full kinetics are estimated by including the collisional ionization and multiphoton rates

$$\dot{N}_e(t) = \alpha I(t) N_e(t) + \sigma_7 I^7(t), \tag{25}$$

where α is the collisional cross section, and σ_7 is the cross section for seven-photon ionization of ethylene glycol at 800 nm (ethylene glycol has a 10.16 eV ionization potential [49]). The multiphoton process injects carriers which are then collisionally excited. Experimentally, material damage is readily observed in liquids at intensities above 10 TW/cm^2, roughly coinciding with N_c. The Keldysh parameter $\gamma=\omega\sqrt{2V}/E$ equals unity at 80 TW/cm^2 marking the border beyond which carrier injection by tunneling ionization must be considered in addition to multiphoton ionization.

It is worth noting that N_c is below the typical density of a liquid (e.g., the density of water is 3.3×10^{22} cm^{-3}), but well above the density of a gas at room temperature and pressure (e.g., an ideal gas density is 2.5×10^{19} cm^{-3}). Therefore in a gas N_e is limited by the number of gas molecules available whereas in a liquid N_e is typically limited by the number of photons available. Thus plasma switching is possible in air, but the efficacy is much less than in a liquid.

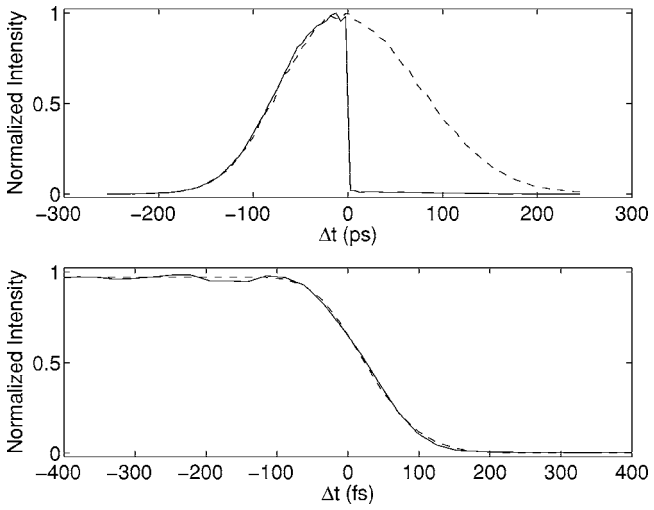

FIG. 4. Optical cross correlation in a 100 μm thick BBO of the switched 1.064 μm pulse with the probe pulse. (Top) Low resolution scan of the unswitched pulse (dashed line) and switched pulse (solid line). (Bottom) High resolution scan of switch showing rapid and complete extinction. The dashed line is the fit to (26) with $\tau_r=150$ ps and $\tau_f=170$ fs.

Characterization of the switched pulse was performed via optical cross correlation in a 100 μm thick BBO crystal with a reference 800 nm pulse (type 1 sum frequency generation). The 800 nm beam's focal diameter in the crystal was larger than that of the 1.064 μm beam in order that the entire beam profile of the switched pulse was cross correlated. A typical cross correlation is shown in Fig. 4.

For a switched laser pulse with a Gaussian intensity rise time τ_r and fall time τ_f, the second order cross correlation function with a probe pulse of Gaussian width τ_p is

$$\begin{aligned} C^{(2)}(\Delta t) &= \int_{-\infty}^{0} e^{-at^2/\tau_r^2} e^{-a(t-\Delta t)^2/\tau_p^2} dt \\ &\quad + \int_{0}^{\infty} e^{-at^2/\tau_f^2} e^{-a\,(t-\Delta t)^2/\tau_p^2)} dt \\ &= \frac{\sqrt{\pi}\tau_r\tau_p e^{-a\Delta t^2/(\tau_p^2+\tau_r^2)}}{2\sqrt{a}\sqrt{\tau_p^2+\tau_r^2}}\left[1 - \mathrm{erf}\left(\frac{\sqrt{a}\tau_r\Delta t}{\tau_p\sqrt{\tau_p^2+\tau_r^2}}\right)\right] \\ &\quad + \frac{\sqrt{\pi}\tau_f\tau_p e^{-a\Delta t^2/(\tau_p^2+\tau_f^2)}}{2\sqrt{a}\sqrt{\tau_p^2+\tau_f^2}}\left[1 + \mathrm{erf}\left(\frac{\sqrt{a}\tau_f\Delta t}{\tau_p\sqrt{\tau_p^2+\tau_f^2}}\right)\right], \end{aligned} \tag{26}$$

where $a=4\ln(2)$ if full-width-at-half-maximum (FWHM) values are used for the time durations. The fit to (26) shown in Fig. 4 indicates that a switched pulse with $\tau_r=150$ ps and $\tau_f=170$ fs has been created. The intense infrared laser pulse has a fall time that is a factor of almost one-thousand times faster than its rise time. No effort was made to manage the

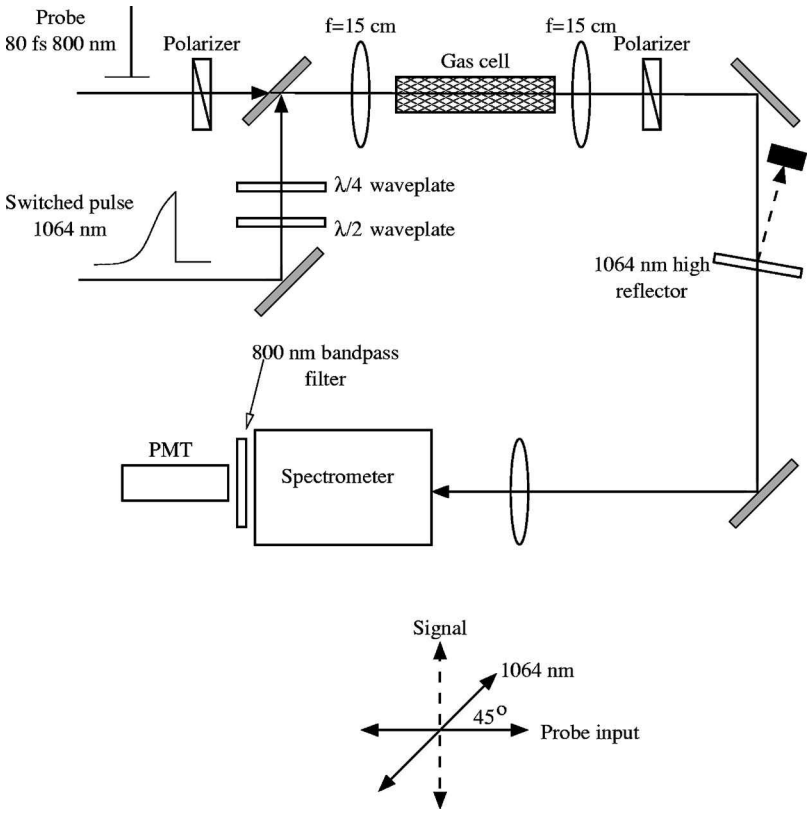

FIG. 5. (top) Optical arrangement for measurement of molecular axis alignment using the optical Kerr effect, and (bottom) the polarization arrangement of the beams.

dispersion of the switched laser pulse as it propagated; it is anticipated that with suitable dispersion control, significantly shorter fall times τ_f would be observed. We note that under appropriate conditions it should be possible to use the light reflected from the plasma to generate a pulse that switches on rapidly and falls slowly.

V. PROBING MOLECULAR AXIS ALIGNMENT WITH THE OPTICAL KERR EFFECT

A. OKE experimental setup

The experimental optical Kerr effect setup is depicted in Fig. 5. Residual scattered 800 nm light copropagating with the 1.064 μm pulse after the plasma shutter was removed using long wave pass dielectric mirrors (see Fig. 3). The switched pump laser pulse was focused into a gas cell containing up to a few hundred Torr of the gas under study. A weak copropagating probe pulse derived from the 800 nm beam was used to probe the evolution of the molecular axis alignment via the optical Kerr effect as a function of time delay after the switch. Since this beam is derived from the 800 nm beam prior to the switch, the probe beam is synchronized to the falling edge of the switched 1.064 μm pulse and is unaffected by jitter between the 800 nm beam and the 1.064 μm beam. The copropagating switched and probe beams were focused into the gas cell with an $f=150$ mm infrared achromatic lens. The beam diameter of the 800 nm probe beam (10 mm) prior to focusing was chosen to be larger than the 1.064 μm beam, such that the smaller focus of the probe beam sampled the highest intensity region of the 1.064 μm focus. Prior to the gas cell, the probe passed through a Glan-Taylor polarizer oriented at +45° clockwise with respect to the switched pulse. Following the gas cell, the probe beam was recollimated with an $f=150$ mm lens and the 800 nm probe energy transmitted through a second crossed polarizer (−45°) after the gas cell was recorded as a function of time delay between the switched and probe pulses ($\Delta t=t_p-\tau_{sw}$). The extinction ratio of the crossed polarizer pair was $<10^{-6}$. The transmitted probe pulse was passed through a 1.064 μm high reflector mirror to remove residual light from the switched pulse and then dispersed in a 0.4 m monochromator. A 800 nm interference filter (25 nm FWHM bandpass) was placed at the exit slit of the monochromator, and the transmitted probe light detected with a photomultiplier tube. The time delay Δt was adjusted via a computer controlled stepper motor translation stage.

B. Optical Kerr effect theory

The application of the switched optical pulse will induce Raman transitions producing microscopic alignment of a sample gas which will result in a macroscopic birefringence. A polarized probe laser beam propagating through the sample will therefore experience an optical rotation which will be dependent upon the degree and direction of the axis alignment of the sample [50]. It is common to describe the process of a Raman excitation followed by a probe in terms of the third order polarizability $\boldsymbol{P}^{(3)}$ [51]. However, if the Raman excitation is nonperturbative, as is the case here, the formalism may fail. Alternatively, if the pump and probe are not overlapped in time, the weak probe pulse may be treated

as propagating in a coherent medium in purely linear way; we consider this situation below.

Consider a weak probe wave with an analytic signal $\boldsymbol{E}_{in}$. For linear birefringence, the rotation of polarization that the probe experiences as it traverses the gas sample can be described by the transfer matrix T

$$\boldsymbol{E}_{in} \rightarrow [1+\mathsf{T}]\boldsymbol{E}_{in}. \tag{27}$$

To determine T note that the phase delay a plane electromagnetic wave receives as it traverses a medium of isotropic refractive index $n=\sqrt{1+4\pi N\alpha}$ is $\phi=(n-1)L\omega/c$, where α is the polarizability, N is the number density, and L is the effective sample thickness. This phase delay is created by interference of the ingoing wave, with the field radiated by the polarization it creates in the medium. T can be calculated directly by considering the dipole radiation from charge oscillations induced in the target or it can be determined from the interference relationship

$$e^{-i\phi}E_{in} = [1+\mathsf{T}]E_{in}, \tag{28}$$

where we find

$$\mathsf{T} = e^{i\phi} - 1. \tag{29}$$

In the limit of small susceptibility,

$$\mathsf{T} \approx \frac{2\pi i\omega NL}{c}\alpha. \tag{30}$$

This relationship holds only for small phase delays ϕ which in practice places a limit on the gas densities that one can employ. For nonisotropic media the transfer matrix generalizes to

$$\mathsf{T}^{ab} \approx \frac{2\pi i\omega NL}{c}\alpha^{ab}, \tag{31}$$

where $\{a,b \in x,y,z\}$.

Experimentally, the induced birefringence is detected by observing the rotation of a probe beam through crossed polarizers (Fig. 3). In the ideal case, a probe beam travels through a polarizer $\hat{\boldsymbol{p}}$, though the sample, and through a second polarizer $\hat{\boldsymbol{s}}$ crossed at a right angle with respect to $\hat{\boldsymbol{p}}$, and then onto a detector whose signal is given by

$$I_1 = |\boldsymbol{E}_{sig}|^2, \tag{32}$$

where

$$\boldsymbol{E}_{sig} = \hat{\boldsymbol{s}}\hat{\boldsymbol{s}} \cdot \mathsf{T} \cdot \hat{\boldsymbol{p}}\hat{\boldsymbol{p}} \cdot \boldsymbol{E}_{in}. \tag{33}$$

Heterodyne detection is achieved by adding an additional field $\boldsymbol{E}_{hetero}$ to the signal $\boldsymbol{E}_{sig}$, and mixing the two on a detector

$$I_2 = |\boldsymbol{E}_{sig} + \boldsymbol{E}_{hetero}|^2. \tag{34}$$

Provided $|\boldsymbol{E}_{sig}| \ll |\boldsymbol{E}_{hetero}|$, the observed signal is

$$I_2 = |\boldsymbol{E}_{hetero}|^2 + 2\Re[\boldsymbol{E}_{hetero}\boldsymbol{E}^*_{sig}]. \tag{35}$$

Above, the first term represents a static positive offset and the second term represents the signal multiplied, and hence amplified, by the heterodyne component. Depending on the relative phases of the signal and heterodyne, the sign of the second term may be negative and the observed detector signal my appear to go negative owing to the static positive offset.

In principle, $\boldsymbol{E}_{hetero}$ may be generated in a number of ways. For linear birefringence, the linear transfer matrix of the whole system R is composed of the time-dependent birefringence of the target $\mathsf{T}(t)$ as well as the static birefringence B_0 between $\hat{\boldsymbol{p}}$ and the target, and the static birefringence B_1 between the target and $\hat{\boldsymbol{s}}$:

$$1+\mathsf{R} = [1+\mathsf{B}_1][1+\mathsf{T}(t)](1+\mathsf{B}_0). \tag{36}$$

It is convenient to decompose R further as

$$\mathsf{R} = \mathsf{T}(t) + \mathsf{U} + \mathsf{V}(t), \tag{37}$$

where $\mathsf{U}=\mathsf{B}_0+\mathsf{B}_1+\mathsf{B}_1\mathsf{B}_0$ is a static contribution and $\mathsf{V}(t)=\mathsf{B}_1\mathsf{T}(t)+\mathsf{T}(t)\mathsf{B}_0+\mathsf{B}_1\mathsf{T}(t)\mathsf{B}_0$ is a time-dependent contribution. The transfer matrix is composed of a sum of the component due to the sample birefringence, $1+\mathsf{T}(t)$, the component due to the static birefringence in the apparatus U, as well as the product of the two $\mathsf{V}(t)$. The signal at a detector is thus

$$I_2 = |\hat{\boldsymbol{s}}\hat{\boldsymbol{s}} \cdot [1+\mathsf{T}(t)+\mathsf{U}+\mathsf{V}(t)] \cdot \hat{\boldsymbol{p}}\hat{\boldsymbol{p}} \cdot \boldsymbol{E}_{in}|^2. \tag{38}$$

Comparing with (34) and (32) we identify

$$\boldsymbol{E}_{hetero} = \hat{\boldsymbol{s}}\hat{\boldsymbol{s}} \cdot [1+\mathsf{U}+\mathsf{V}(t)] \cdot \hat{\boldsymbol{p}}\hat{\boldsymbol{p}} \cdot \boldsymbol{E}_{in}. \tag{39}$$

To recover the ideal (homodyne) case there are two conditions that must be met: (i) The polarizers must be crossed $\hat{\boldsymbol{s}} \cdot \hat{\boldsymbol{p}} = 0$ and (ii) there can be no birefringence in the intervening optics B_0, $B_1=0$. Thus, one may induce heterodyne detection by either slightly rotating a polarizer or, alternatively, inducing some material birefringence.

It should be noted that the derived detector signals differ from the occasionally used formula $I \propto |\boldsymbol{E}_{sig}+\text{const}|^2$ in that they may contain a time-dependent offset arising from compound rotations [i.e., $V(t)$] when (ii) is not satisfied.

We consider now the specific case of probing the alignment induced by a linearly polarized laser field propagating along $\hat{\mathbf{x}}$ and polarized in the $\hat{\mathbf{z}}$ direction. We consider a copropagating probe laser field linearly polarized at 45° to the aligning field

$$\mathbf{E}_{in} = \frac{E_0}{\sqrt{2}}(\hat{\mathbf{z}}+\hat{\mathbf{y}})e^{-i\omega t}. \tag{40}$$

The signal field is detected by a analyzing polarizer at 90° to the input probe field polarization direction such that $\hat{\mathbf{s}}$ is defined by

$$\hat{\mathbf{s}} = \frac{1}{\sqrt{2}}(\hat{\mathbf{z}}-\hat{\mathbf{y}}). \tag{41}$$

Equations (31), (32), (40), and (41) may be used with to describe the homodyne signal

$$I_1(t) = |\hat{\mathbf{s}} \cdot \mathsf{T}(t) \cdot \mathbf{E}_{in}|^2 \propto \langle \alpha^{zz} - \alpha^{yy} \rangle^2, \tag{42}$$

where quantum expectation values are denoted by angled brackets. Relating the laboratory frame polarizability

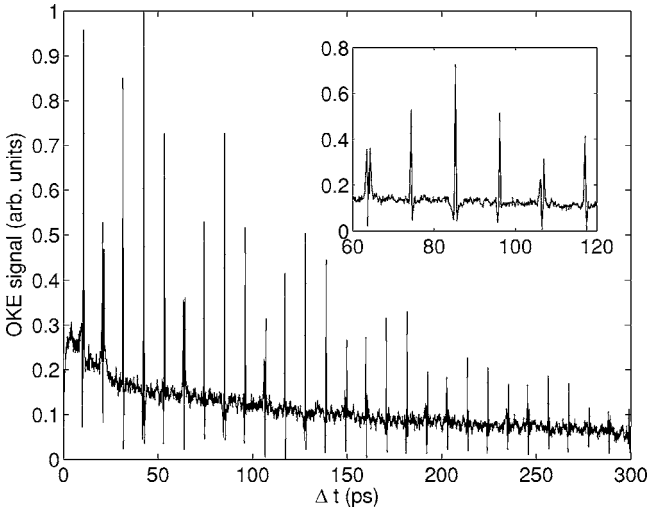

FIG. 6. The switched wave packet optical Kerr effect signal from carbon dioxide at 300 Torr and 300 K. Wave packet revivals are seen with a spacing of $\Delta T = 1/8B = 10.7$ ps.

components in (42) to the molecular frame polarizability components (using direction cosine matrix elements [41]) gives

$$I(t) \propto \left[\langle \cos^2 \theta \rangle(t) - \tfrac{1}{3}\right]^2, \tag{43}$$

where the expectation value $\langle \cos^2 \theta \rangle$ is a measure of molecular axis alignment. This expectation value takes a value of $\frac{1}{3}$ for a randomly oriented ensemble of molecules, for which the birefringence and the signal will be zero. It is clear from this equation that the observed signal will reflect the molecular axis alignment.

VI. EXPERIMENTAL RESULTS

In Figs. 6–8 we show the experimental creation of switched rotational wave packets at 300 K for two linear molecules, carbon dioxide (CO_2) and carbon disulphide (CS_2), and a polyatomic prolate symmetric top molecule, 1,2-propadiene (C_3H_4). Following the truncation of the switched 1.064 μm alignment pulse (at $\Delta t = 0$ ps), clear rotational wave packet revivals are seen with associated field-free molecular axis alignment. In all three cases the signal intensity is seen to reduce with time due to collisional decoherence. Uncompensated static birefringence from the optical elements in the apparatus resulted in a degree of heterodyning of the signal for the carbon dioxide and 1,2-propadiene data, as evidenced by the apparently negative excursion of the signal. Conversely, the effects of static birefringence were removed from the carbon disulphide experiments resulting in a positive going homodyne signal.

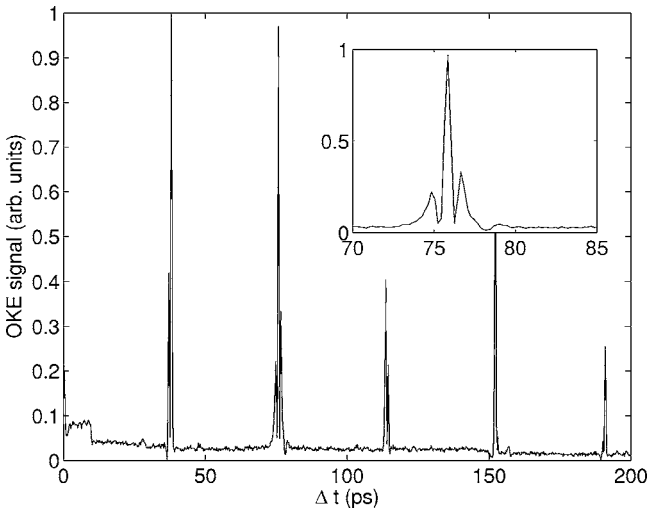

FIG. 7. The switched wave packet optical Kerr effect signal in carbon disulphide at 300 Torr and 300 K. Wave packet revivals are seen with a spacing of $\Delta T = 1/8B = 38$ ps.

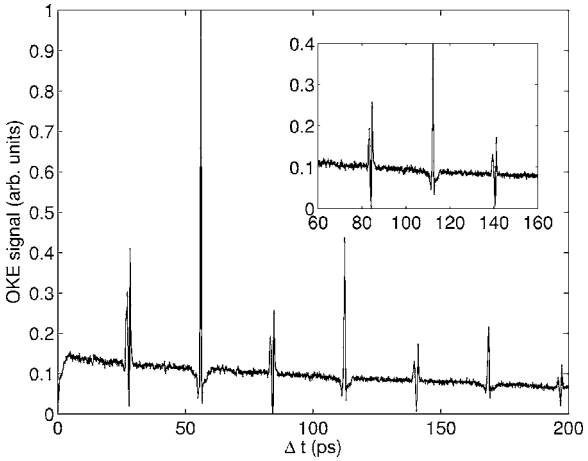

FIG. 8. The optical Kerr effect signal in 1,2-propadiene at 200 Torr and 300 K. Wave packet revivals are seen with a spacing of $\Delta T = 1/8B = 28.1$ ps.

Although the potential well depth created by the 1.064 μm laser field in these experiments was small (<1 cm^{-1}) compared to the thermal energy of the molecules at $T = 300$ K ($kT = 208$ cm^{-1}), resulting in a low degree of molecular axis alignment, the observed wave packet behavior clearly demonstrates the utility of this approach to the nonresonant control over molecular motion, in this case rotational motion and molecular axis alignment.

The revival structure reflects the field-free energy level spacing of the molecules and so carries spectroscopic and structural information. In order to understand the coherences which are responsible for the observed signals, we need to examine the matrix elements of $\cos^2 \theta$ which appear in (22) and (43). This is most conveniently achieved by employing the symmetric top rotational basis, which are specified in terms of the quantum numbers for the angular momentum J, its projection upon the LF z axis (in this case, the aligning laser field polarization direction) M, and K which denotes the projection of $\mathbf{J}$ upon the molecular frame z axis [41]. For linear molecules, we need to consider $K = 0$ only, whereas for symmetric top molecules $K = -J, \ldots, J$. The matrix elements of the $\cos^2 \theta$ operator between symmetric top basis functions may be expressed in terms of Wigner 3-j coefficients as

$$\langle J'M'K'|\cos^2\theta|JKM\rangle = \frac{\delta_{MM'}\delta_{KK'}}{3}\left[1+2(2J+1)^{1/2}(2J'+1)^{1/2}\times\begin{pmatrix}J' & 2 & J\\ M & 0 & -M\end{pmatrix}\begin{pmatrix}J' & 2 & J\\ K & 0 & -K\end{pmatrix}\right], \tag{44}$$

where, from the properties of the Wigner 3-j coefficients, $J'=J,J\pm2$. The expressions for a linear molecule are included as an Appendix. From this equation it is apparent that the OKE signal results from coherences between states with $\Delta J=0,\pm2$, $\Delta M=0$, and $\Delta K=0$. In the terminology often used in the context of rotational coherence spectroscopy, the modulation of the OKE signal arises due to J type coherences [52,53].

The expectation value $\langle\cos^2\theta\rangle(t)$ in (43) is an average of the expectation values $\langle\cos^2\theta\rangle_{N_0}(t)$ of the thermally populated initial states $N_0=J_0K_0M_0$

$$\langle\cos^2\theta\rangle(t)=\sum_{N_0}W_{N_0}\langle\cos^2\theta\rangle_{N_0}(t), \tag{45}$$

where W_{N_0} is the Boltzmann weighting. Each initially populated state is transformed into a superposition of rotational states by the alignment field, represented by

$$|\Psi(t)\rangle_{N_0}=\sum_{JKM}A^{N_0}_{JKM}(t)e^{i\Phi^{N_0}_J(t)}e^{-iE_{JK}t/\hbar}|JKM\rangle, \tag{46}$$

where the sums over K and M are restricted to $K=K_0$ and $M=M_0$ and $A^{N_0}_{JKM}(t)$ is defined to be real. The expectation value $\langle\cos^2\theta\rangle_{N_0}(t)$ is then given by

$$\langle\cos^2\theta\rangle_{N_0}(t)=\sum_{JKM}\{[A^{N_0}_{JKM}(t)]^2M^{KM}_{J,J}+2A^{N_0}_{JKM}(t)A^{N_0}_{J+2KM}(t)M^{KM}_{JJ+2}\times\cos[\Delta\omega_{JK}t+\Delta\Phi^{N_0}_{JKM}(t)]\}, \tag{47}$$

where $M^{K_0M_0}_{J,J'}$ are the matrix elements of $\cos^2\theta$

$$M^{K_0M_0}_{J,J'}=\langle JK_0M_0|\cos^2\theta|J'K_0M_0\rangle, \tag{48}$$

which are defined in (44) above. The frequency components of (47) are given in terms of the energy separations of the field free rotational energy levels

$$\Delta\omega_{JK}=\frac{E_{J+2K}-E_{JK}}{\hbar}. \tag{49}$$

The phase factors in (47) are defined as

$$\Delta\Phi^{N_0}_{JKM}(t)=\Phi^{N_0}_{JKM}(t)-\Phi^{N_0}_{J+2KM}(t). \tag{50}$$

When the alignment laser field is adiabatically turned on the phases $\Phi^{N_0}_J(t)$ remain equal at all times such that all $\Delta\Phi^{N_0}_{JKM}(t)=0$. This also implies that the components of the signal arising from different initially populated states N_0 are all in phase. This is in contrast to impulsive alignment with short laser pulses, where the nonadiabatic nature of the interaction gives nonuniform distribution of phases $\Phi^{N_0}_J(t)$ [23,54]. Following the sudden truncation of the alignment field, the field induced wave packet is projected onto the field free basis, and the $A^{N_0}_{JKM}(t)$ and $\Phi^{N_0}_J(t)$ remain constant with time. The subsequent evolution of $\langle\cos^2\theta\rangle(t)$ is then given by

$$\langle\cos^2\theta\rangle(t)=\sum_{JKM}[\mathcal{A}^2_{JKM}M^{KM}_{JJ}+2\mathcal{B}_{JKM}M^{KM}_{JJ+2}\cos(\Delta\omega_{JK}t)], \tag{51}$$

where we have defined $t=0$ as the time when the alignment field was truncated, and

$$\mathcal{A}^2_{JKM}\equiv\sum_{N_0}W_{N_0}(A^{N_0}_{JKM})^2 \tag{52}$$

and

$$\mathcal{B}_{JKM}\equiv\sum_{N_0}W_{N_0}A^{N_0}_{JKM}A^{N_0}_{J+2KM}. \tag{53}$$

The rotational energy of linear molecules, in this case carbon dioxide and carbon disulphide, is given by $E_J=BJ(J+1)$ in the rigid-rotor limit and so $\Delta\omega_{J,J+2}=2B(2J+3)/\hbar$. This would lead to revivals in $\langle\cos^2\theta\rangle(t)$ with spacing $1/(4B)$ (corresponding to one quarter of the classical rotational period). However the nuclear statistics for these two molecules result in only even J levels being present and revivals with spacing $1/(8B)$. The observed spacing between revivals of 10.7 ps for carbon dioxide and 38.0 ps for carbon disulphide agree well with the known values of B [55]. Furthermore, as shown in Figs. 9 and 10, taking a Fourier transform of the OKE signal after the truncation of the alignment pulse yields a rotational spectrum of the molecule. In both of these spectra clearly resolved lines spaced by $8B$ are observed. However, close examination of the spectra reveals more than one progression of lines. Evaluating the square in (43) yields the following expression

$$I(t)\propto[\langle\cos^2\theta\rangle(t)]^2+\tfrac{2}{3}\langle\cos^2\theta\rangle(t)+\tfrac{1}{9}. \tag{54}$$

From (51) we find

$$[\langle\cos^2\theta\rangle(t)]^2=\sum_{JKM}\sum_{J'K'M'}[\mathcal{A}^2_{JKM}M^{KM}_{JJ}\mathcal{A}^2_{J'K'M'}M^{K'M'}_{J'J'}+4\mathcal{A}^2_{JKM}M^{KM}_{JJ}\mathcal{B}_{J'K'M'}M^{K'M'}_{J'J'+2}\cos(\Delta\omega_{J'K'}t)+4\mathcal{B}_{JKM}M^{KM}_{JJ+2}\mathcal{B}_{J'K'M'}M^{K'M'}_{J'J'+2}\cos(\Delta\omega_{JK}t)\times\cos(\Delta\omega_{J'K'}t)]. \tag{55}$$

Noting that the third term in this expression contains the products

$$\cos(\Delta\omega_{JK}t)\cos(\Delta\omega_{J'K'}t)=\tfrac{1}{2}\cos(\Delta\omega_{JK}t+\Delta\omega_{J'K'}t)+\tfrac{1}{2}\cos(\Delta\omega_{JK}t-\Delta\omega_{J'K'}t), \tag{56}$$

we see that there are three progressions of frequencies contributing to the OKE signal. In addition to the fundamental frequencies $\Delta\omega_{JK}$, there are sum and difference frequencies, $(\Delta\omega_{JK}+\Delta\omega_{J'K'})$ and $(\Delta\omega_{JK}-\Delta\omega_{J'K'})$ respectively. While these sum and difference frequencies will have the same

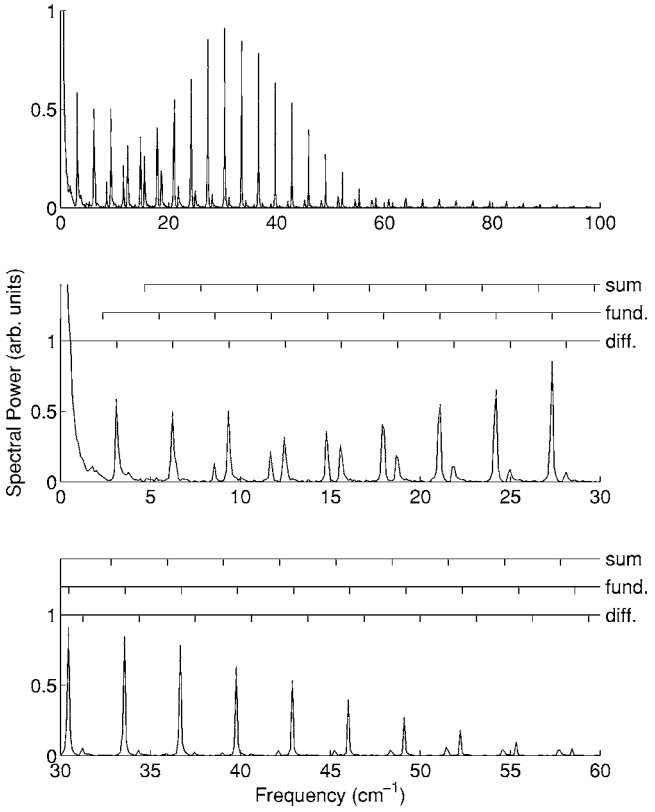

FIG. 9. Fourier transform of the optical Kerr effect signal from CO_2 at 300 torr and 300 K. Combs indicating progressions of lines corresponding to the fundamental, difference, and sum frequencies are shown in the lower plots. Each progression consists of lines with a measured spacing corresponding to $8B$, with $B=0.3906$ cm^{-1} taken from Ref. [55].

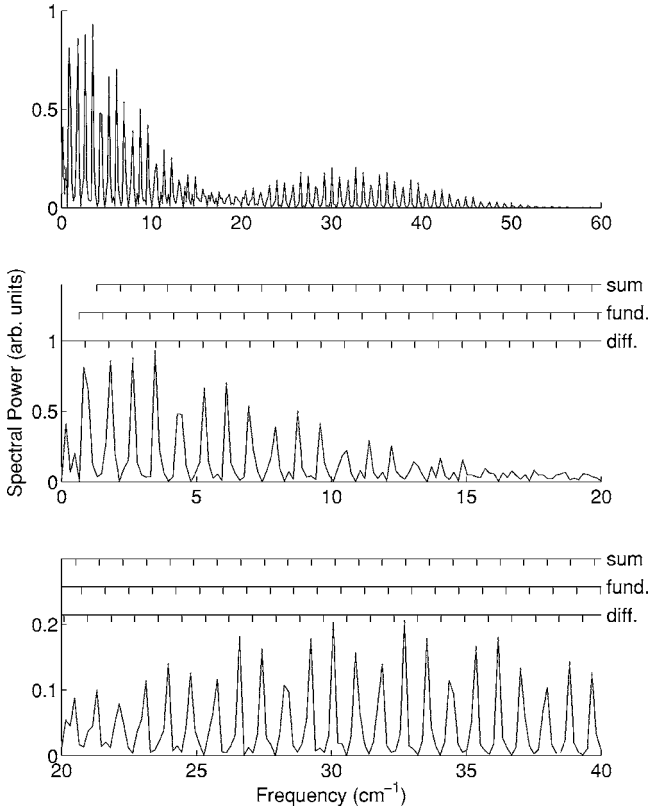

FIG. 10. Fourier transform of the optical Kerr effect signal from CS_2 at 300 torr and 300 K (Fig. 7). Combs indicating progressions of lines corresponding to the fundamental, difference, and sum frequencies are shown in the lower plots. These frequency combs have a spacing of $8B$, with the value $B=0.1092$ cm^{-1} taken from Ref. [55].

spacing as the fundamental frequencies, they will be off set in value. In general, for a linear molecule, the difference frequency components will be at $4JB=0,4B,8B,\ldots$, the fundamental frequency components will be at $(4J+6)B=6B,10B,14B,\ldots$, and the sum frequency components will be at $(4J+4J'+12)B=12B,16B,20B,\ldots$, where $J,J'\in\mathbb{Z}^*$. Above a frequency of $12B$, the sum and difference frequency components take the same value. For carbon dioxide and carbon disulphide which have only even J levels the difference frequency components will be at $8JB=0,8B,16B,\ldots$, the fundamental frequency components will be at $(8J+6)B=6B,14B,22B,\ldots$, and the sum frequency components will be at $(8J+8J'+12)B=12B,20B,28B,\ldots$. For these two molecules, the sum and difference frequencies do not coincide. These progressions of lines are seen clearly in Figs. 9 and 10, where the spacings between the lines agree well with the known values of the rotational constants for these molecules [55]. This clearly demonstrates the suitability of this technique for ground state rotational spectroscopy. Compared with microwave spectroscopy, traditionally used to perform rotational spectroscopy of ground state molecules, this method has a number of benefits: there is no requirement to tune either laser to resonance with the rotational transitions, the molecules does not need to possess a permanent dipole moment, and the technique is inherently free of Doppler broadening. Furthermore, since many rotational states may in principle comprise the rotational wave packet, more lines in the recovered rotational spectrum are obtained than would be accessible from dipole allowed transitions, which are subject to more restrictive selection rules.

In Fig. 8 we show the OKE signal demonstrating the creation of a switched rotational wave packet for the polyatomic molecule 1,2-propadiene, a prolate symmetric top molecule. The rotational energy a rigid-rotor prolate symmetric top is given in terms of two rotational constants A and C as $E_{JK}=CJ(J+1)+(A-C)K^2$. Here A is the rotational constant for rotation about the figure axis (which has the lowest moment of inertia), and C is the rotational constant for rotation perpendicular to the figure axis. Since $\cos^2\theta$ is diagonal in K [see (44)], only states with the same value of K are coupled by the aligning laser field, and the wave packet will contain frequency components spaced by $4C$, with wave packet revivals spaced by $1/(4C)$. The fact that the second rotational constant, A, does not affect the revival structure is because rotation about the figure axis does not affect the value of θ(the angle between the figure axis and the polarization direction of the aligning field), and so does not affect the molecular axis alignment. The OKE signal therefore contains no information regarding rotation about the figure axis of the molecule. In comparison with other methods for rotational

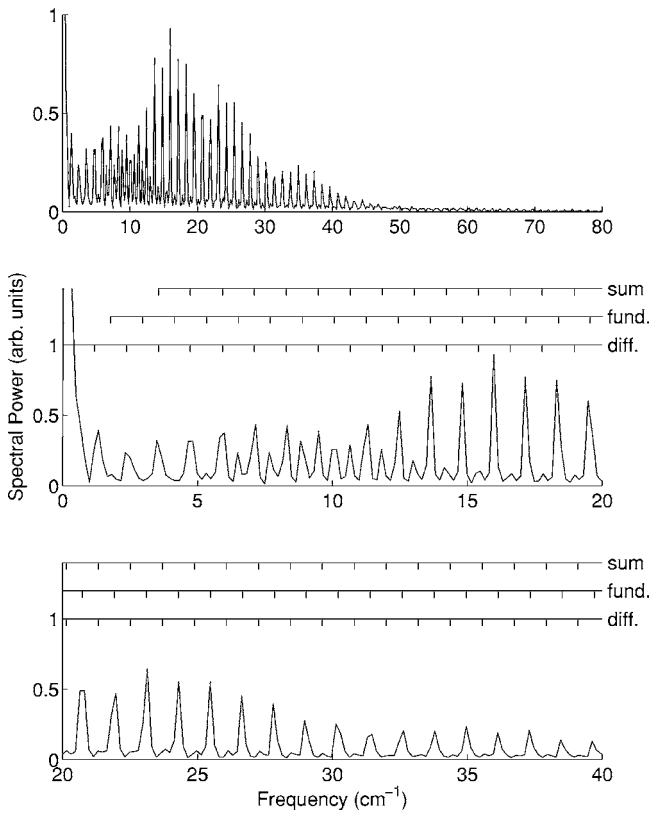

FIG. 11. Fourier transform of the optical Kerr effect signal from 1,2-propadiene at 200 torr and 300 K (Fig. 8). Combs indicating progressions of lines corresponding to the fundamental, difference, and sum frequencies are shown in the lower plots. These frequency combs have a spacing of $4C$, with the value of $C=0.2963$ cm^{-1} taken from Ref. [63].

coherence spectroscopy, the experimental geometry described here is sensitive to *J*-type coherence, but not *K*-type coherence. Following similar argumentation for linear molecules above, three sets of frequency components contribute to the observed signal, as show in the Fourier transform of the OKE signal (Fig. 11). The difference frequency components will be at $4JC=0,4C,8C,\ldots$, the fundamental frequency components will be at $(4J+6)C=6C,10C,14C,\ldots$, and the sum frequency components will be at $(4J+4J'+12)C=12C,16C,20C,\ldots$. We note that the sum and difference frequency components will take the same values at $12C$ and above.

VII. CONCLUSION

Electric forces underlie essentially all of molecular and solid state physics and therefore it seems natural to use strong, highly controlled electric fields to control such systems. As all charged quantum systems have a Stark response, we therefore believe the NRDSE technique should find general applicability.

We have considered a quantum control scenario involving the nonresonant dynamic Stark effect as induced by shaped intense femtosecond infrared laser fields. This method applies to the intermediate field strength regime where the interaction is nonperturbative but nonionizing. In this regime, the nature of the control can be understood as dynamic but reversible modification of an effective propagator (effective Hamiltonian) during the system propagation. The NRDSE method has recently been applied to the control of vibrational and predissociation dynamics in a diatomic molecule [21]. Here we chose a different example of this type of control, namely the generation of unique field-free states via adiabatic application and sudden truncation of the NRDSE, thus generating switched wave packets.

For the particular case of molecular rotations, NRDSE manifests itself as a molecular axis alignment: the field-free potential, being flat, is dynamically modified to produce a potential well along the field polarization direction. Following rapid truncation of the laser field, switched molecular rotational wave packets are created. Using the optical Kerr effect as a probe, switched rotational wave packets were experimentally demonstrated in the linear polyatomic molecules CO_2 and CS_2, and the nonlinear polyatomic molecule 1,2-propadiene (C_3H_4). The subsequent field-free wave packet evolution provides very detailed information about molecular structure: it is a completely nonresonant form of rotational coherence spectroscopy with no *a priori* information about the molecular system being required in order to extract the rotational constants. Extensions to full, three-dimensional alignment of general polyatomic molecules may be achieved through the use of elliptically polarized fields or with the assistance of a compound kick method [56].

There has also been considerable interest in studies of rotational decoherence [57–59]. We directly observed the dephasing of rotational coherences due to collisions with the ambient background gas. By nonresonantly generating rotational coherences and monitoring their evolution as a function of background pressure, the switched wave packet technique will be able to directly investigate rotational decoherence. In addition, kicking the rotor with an infrared femtosecond pulse while the strong field is on (i.e., before the switch off) will allow the creation of pendular wave packets and the formation of squeezed states of the rotor [60,61]. Furthermore, switched rotors also provide an opportunity to create precisely selected birefringence for applications where high-speed time-dependent phase control is required.

Advances in field-free molecular alignment and orientation will only become more important with time. For investigations of molecular structure, alignment will provide the opportunity to make increasingly differential measurements. As a method of microscopic quantum control it will provide the first step for alignment dependent chemistry. The switched wave packet technique is not limited to alignment alone, however. It can be applied to all degrees of freedom that couple to optical fields and it offers control without significant knowledge of the target system. For example, the only prerequisite is that the pulse rise time is sufficiently long to be adiabatic and that the pulse fall time must be much shorter than the characteristic motion time scale. As studies scale to larger molecules and more diverse systems, these characteristic of general applicability for control techniques will become essential if quantum control

methods are to be implemented in a truly widespread and effective manner.

ACKNOWLEDGMENTS

The authors gratefully acknowledge helpful discussions with D. M. Villeneuve, P. B. Corkum, and D. M. Rayner. Additionally we acknowledge the invaluable help of Jeff Mottershead. J.G.U. acknowledges a British Council-NRC Researcher Exchange Award and EPSRC support under grant EP/C530756/1. We also acknowledge support from NSERC.

APPENDIX: MATRIX ELEMENTS OF $\cos^2(\theta)$ FOR LINEAR MOLECULES

The matrix elements of $\cos^2(\theta)$ for linear molecules have been incorrectly reported in the literature and are included here for convienience. They can be obtained, for example, from the spherical harmonic recurrence relations [62]

$$\begin{aligned}\langle J'M'|\cos^2(\theta)|JM\rangle = \delta_{M'M}[&\delta_{J',J-2}D^M_{J-1}D^M_J \\ &+ \delta_{J',J}((D^M_{J+1})^2 + (D^M_J)^2) \\ &+ \delta_{J',J+2}D^M_{J+1}D^M_{J+2}],\end{aligned} \tag{A1}$$

where

$$D^M_J = \sqrt{\frac{(J-M)(J+M)}{(2J-1)(2J+1)}}. \tag{A2}$$

[1] P. W. Brumer and M. Shapiro, *Principles of the Quantum Control of Molecular Processes* (Wiley-Interscience, New Jersey, 2003).
[2] S. A. Rice and M. Zhao, *Optical Control of Molecular Dynamics* (John Wiley and Sons, New York, 2000).
[3] P. Brumer and M. Shapiro, Annu. Rev. Phys. Chem. **43**, 257 (1992); and references therein.
[4] R. J. Gordon and S. A. Rice, Annu. Rev. Phys. Chem. **48**, 601 (1997); and references therein.
[5] U. Gaubatz, P. Rudecki, S. Schiemann, and K. Bergman, J. Chem. Phys. **92**, 5363 (1990).
[6] K. Bergmann, H. Theuer, and B. W. Shore, Rev. Mod. Phys. **70**, 1003 (1998).
[7] A. Shnitman, I. Sofer, I. Golub, A. Yogev, M. Shapiro, Z. Chen, and P. Brumer, Phys. Rev. Lett. **76**, 2886 (1996).
[8] R. S. Judson and H. Rabitz, Phys. Rev. Lett. **68**, 1500 (1992).
[9] A. Assion, T. Baumert, M. Bergt, T. Brixner, B. Kiefer, V. Seyfried, M. Strehle, and G. Gerber, Science **282**, 919 (1998).
[10] R. J. Levis, G. M. Menkir, and H. Rabitz, Science **292**, 709 (2001).
[11] M. Strehle and G. Gerber, AIP Conf. Proc. **525**, 295 (2000).
[12] E. Constant, H. Stapelfeldt, and P. B. Corkum, Phys. Rev. Lett. **76**, 4140 (1996).
[13] A. D. Bandrauk, ed., *Molecules in Laser Fields* (Marcel Dekker, Inc., New York, 1994).
[14] M. Lezius, V. Blanchet, D. M. Rayner, D. M. Villeneuve, A. Stolow, and M. Y. Ivanov, Phys. Rev. Lett. **86**, 51 (2001).
[15] H. Stapelfeldt, E. Constant, and P. B. Corkum, Phys. Rev. Lett. **74**, 3780 (1995).
[16] T. Brixner, N. H. Damrauer, P. Niklaus, and G. Gerber, Nature (London) **414**, 57 (2001).
[17] B. J. Pearson, J. L. White, T. C. Weinacht, and P. H. Bucksbaum, Phys. Rev. A **63**, 063412 (2001).
[18] D. Meshulach and Y. Silberberg, Phys. Rev. A **60**, 1287 (1999).
[19] V. V. Lozovoy, I. Pastirk, K. A. Walowicz, and M. Dantus, J. Chem. Phys. **118**, 3187 (2003).
[20] J. G. Underwood, M. Spanner, M. Y. Ivanov, J. Mottershead, B. J. Sussman, and A. Stolow, Phys. Rev. Lett. **90**, 223001 (2003).
[21] B. J. Sussman, M. Y. Ivanov, and A. Stolow, Phys. Rev. A **71**, 051401(R) (2005).
[22] B. Friedrich and D. Herschbach, Phys. Rev. Lett. **74**, 4623 (1995).
[23] H. Stapelfeldt and T. Seideman, Rev. Mod. Phys. **75**, 543 (2003).
[24] A. Stolow, Annu. Rev. Phys. Chem. **54**, 89 (2003).
[25] J. G. Underwood and K. L. Reid, J. Chem. Phys. **113**, 1067 (2000).
[26] Y. I. Suzuki, M. Stener, and T. Seideman, Phys. Rev. Lett. **89**, 233002 (2002).
[27] R. Neutze, R. Wouts, D. van der Spoel, E. Weckert, and J. Hajdu, Nature (London) **406**, 752 (2000).
[28] J. C. H. Spence and R. B. Doak, Phys. Rev. Lett. **92**, 198102 (2004).
[29] J. Miao, K. O. Hodgson, and D. Sayre, Proc. Natl. Acad. Sci. U.S.A. **98**, 6641 (2001).
[30] J. C. Williamson, J. Cao, H. Ihee, H. Frey, and A. H. Zewail, Nature (London) **386**, 159 (1997).
[31] H. Niikura, F. Légaré, R. Hasbani, A. D. Bandrauk, M. Y. Ivanov, D. M. Villeneuve, and P. B. Corkum, Nature (London) **417**, 917 (2002).
[32] S. Chelkowski, P. B. Corkum, and A. D. Bandrauk, Phys. Rev. Lett. **82**, 3416 (1999).
[33] R. Velotta, N. Hay, M. B. Mason, M. Castillejo, and J. P. Marangos, Phys. Rev. Lett. **87**, 183901 (2001).
[34] M. Lein, P. P. Corso, J. P. Marangos, and P. L. Knight, Phys. Rev. A **67**, 023819 (2003).
[35] J. Itatani, J. Levesque, D. Zeidler, H. Niikura, H. Pépin, J. C. Kieffer, P. B. Corkum, and D. M. Villeneuve, Nature (London) **432**, 867 (2004).
[36] R. A. Bartels, N. L. Wagner, M. D. Baertschy, M. M. Murnane, and H. C. Kapteyn, Opt. Lett. **28**, 346 (2003).
[37] R. A. Bartels, T. C. Weinacht, N. Wagner, M. Baertschy, C. H. Greene, M. M. Murnane, and H. C. Kapteyn, Phys. Rev. Lett. **88**, 013903 (2001).
[38] B. W. Shore, *The Theory of Coherent Atomic Excitation*, Vol. I and II (Wiley, New York, 1990).
[39] G. L. Peterson and C. D. Cantrell, Phys. Rev. A **31**, 807 (1985).

[40] A. Messiah, *Quantum Mechanics* (North-Holland Publication, Amsterdam, 1962).
[41] R. N. Zare, *Angular Momentum* (John Wiley and Sons, New York, 1988).
[42] A. M. Weiner, Rev. Sci. Instrum. **71**, 1929 (2000).
[43] D. M. Villeneuve, S. A. Aseyev, A. Avery, and P. B. Corkum, Appl. Phys. B: Lasers Opt. **74**, S157 (2002).
[44] A. J. Alcock, P. B. Corkum, and D. J. James, Appl. Phys. Lett. **27**, 680 (1975).
[45] K. Michelmann, A. Glaß, T. Feurer, R. Sauerbrey, and G. Szabó, Appl. Phys. B **71**, 487 (2000).
[46] J. E. Bernard and A. J. Alcock, Opt. Lett. **19**, 1861 (1994).
[47] L. N. Gaier, M. Lein, M. I. Stockman, P. L. Knight, P. B. Corkum, M.-Y. Ivanov, and G. L. Yudin, J. Phys. B **37**(3), L57 (2004).
[48] B. C. Stuart, M. D. Feit, A. M. Rubenchik, B. W. Shore, and M. D. Perry, Phys. Rev. Lett. **74**, 2248 (1995).
[49] *CRC Handbook of Chemistry and Physics*, edited by D. R. Lide (CRC Press, Boca Raton, 2001).
[50] V. Renard, M. Renard, S. Guérin, Y. T. Pashayan, B. Lavorel, O. Faucher, and H. R. Jauslin, Phys. Rev. Lett. **90**, 153601 (2003).
[51] M. Morgen, W. Price, P. Ludowise, and Y. Chen, J. Chem. Phys. **102**, 8780 (1995).
[52] P. W. Joireman, L. L. Connell, S. M. Ohline, and P. M. Felker, J. Chem. Phys. **96**, 4118 (1992).
[53] C. Riehn, Chem. Phys. **283**, 297 (2002).
[54] F. Rosca-Pruna and M. J. J. Vrakking, Phys. Rev. Lett. **87**, 153902 (2001).
[55] G. Herzberg, *Electronic Spectra and Electronic Structure of Polyatomic Molecules* (Van Nostrand, New York, 1966).
[56] J. G. Underwood, B. J. Sussman, and A. Stolow, Phys. Rev. Lett. **94**, 143002 (2005).
[57] S. Wallentowitz, I. A. Walmsley, L. J. Waxer, and T. H. Richter, J. Opt. B: Quantum Semiclassical Opt. **35**, 1967 (2002).
[58] A. Adelswd and S. Wallentowitz, J. Opt. B: Quantum Semiclassical Opt. **6**, S147 (2004).
[59] C. Meier, Phys. Rev. Lett. **93**, 173003 (2004).
[60] I. S. Averbukh and R. Arvieu, Phys. Rev. Lett. **87**, 163601 (2001).
[61] M. Leibscher, I. S. Averbukh, and H. Rabitz, Phys. Rev. Lett. **90**, 213001 (2003).
[62] G. B. Arfken and H. J. Weber, *Mathematical Methods for Physicists* (Academic Press, San Diego, 1995), 4th edition.
[63] N. A. F. Hegelund and M. Koivusaari, J. Mol. Spectrosc. **149**, 305 (1991).